ChemPubSoc Europe

DOI: 10.1002/ejoc.201901736

EurJOC European Journal of Organic Chemistry

Full Paper

Check for updates

Electron Affinity

# Synthesis and Properties of Azadipyrromethene-Based Complexes with Nitrile Substitution

Chunlai Wang,[a] Cassie Daddario,[a] Sandra Pejić,[a] and Geneviève Sauvé*[a]

**Abstract:** Azadipyrromethene (ADP)-based complexes have gained interest due to their strong absorption in the visible to near-IR region and high electron affinity. Attempts to increase their electron accepting properties by electron withdrawing group substitutions have been limited. We previously found that substitution with fluorine at the *p*-distal phenyls or at the *p*-pyrrolic-phenylethynyls of ADP do not shift reduction potentials and thus have no effect on electron affinity. This could be because fluorine also acts as pi-donor, thus, a pi-acceptor substituent may have a greater impact on the energy levels. To test this hypothesis, we synthesized three new ADP-based complexes with nitrile substitutions. Cyclic voltammetry shows that the nitrile substitutions indeed anodically shifts the reduction potentials, leading to increased electron affinity. The shift was ≈ 0.3 V for the *p*-distal phenyl substitution and 0.16V for the *p*-phenylethynyl substitution. Nitrile substitution was also found to improve electron accepting ability and electron mobility in diodes, as compared to the un-substituted analogues.

## Introduction

Azadipyrromethenes (ADPs, Figure 1) are a class of monoanionic bidentate ligands with strong absorption in the visible and near IR range and low reduction potentials.[1] Their optical properties have been tuned through structural modifications and chelation.[1a,2] The most studied systems are $BF_2^+$ chelates, with applications in photodynamic therapy, bio-imaging and light harvesting. Several $BF_2^+$ chelated ADPs and their derivatives were demonstrated as promising donor materials when paired with fullerene ($C_{60}$) as electron acceptor in organic photovoltaics (OPVs).[3] We have previously demonstrated that homoleptic zinc(II) complexes of azadipyrromethenes are promising candidates as non-fullerene acceptors for solution-processed OPV applications.[4] The presence of pyrrolic substituents, such as phenylethynyls in $Zn(WS3)_2$ (Figure 1), combined with the distorted tetrahedral molecular shape of the complex helps tune self-aggregation and enable favorable phase separation from regioregular poly(3-hexylthiophene) (P3HT), resulting in good performance in OPVs.[5] However, the energy levels of $Zn(WS3)_2$ are a bit too high, thus limiting its application as an electron acceptor.

To lower the energy levels of $Zn(WS3)_2$, we explored fluorination at various positions on the ADP ligand: at the *p*-distal phenyl, *p*-proximal phenyl and *p*-pyrrolic phenylethynyls, **A**–**D** in Figure 1.[6] Interestingly, we found that fluorination had very little effect on the redox properties and corresponding estimated HOMO/LUMO energy levels. Fluorine substitution at the *p*-distal phenyls or the *p*-pyrrolic phenylethynyl did not lower the LUMO energy level of $Zn(WS3)_2$ and had little impact on the HOMO energy levels. Amin et al. also found that attaching fluorine to the *p*-distal phenyls of ADP, **E** in Figure 1, did not lower the energy levels of the $BF_2^+$ chelate.[7] On the other hand, addition of –F at the proximal phenyls (**C**) or $-CF_3$ at the pyrrolic phenylethynyls (**D**) of $Zn(WS3)_2$ decreased of the energy levels by 0.09–0.10 eV.[6] When tested in organic solar cells with P3HT as the electron donor, all fluorinated compounds except for **C** (with *p*-proximal phenyl-F) performed better than $Zn(WS3)_2$,[6a] showing that fluorination was nevertheless beneficial for OPV applications. Additionally, fluorination was found to be beneficial for increasing electron mobility.

The fact that fluorination at the *p*-distal phenyl and *p*-proximal phenylethynyls had no effect on the redox properties and corresponding estimated energy levels was surprising to us, since fluorine is routinely used to lower energy levels of conjugated systems due to its high electronegativity.[8] One potential reason for our surprising results is that fluorine can also behave as pi-donor, thus negating its inductive electron withdrawing effect.[9] This motivated us to explore an alternative electron withdrawing group that does not have pi-donating properties: nitriles. Nitriles are highly polar groups that can also behave as pi-acceptors. Nitrile substitution has been demonstrated to lower the energy levels of conjugated molecules and ADP dyes. For example, pentacene's HOMO and LUMO energy levels decreased with the number of nitrile groups incorporated.[10] Jiao et al. attached nitrile groups on the *p*-distal phenyl rings and methoxy groups on the *p*-proximal phenyl rings, **F** in Figure 1.[11] Unlike fluorine,[7] DFT calculations indicate that nitrile groups on the *p*-distal phenyl decrease both the HOMO and

[a] *Department of Chemistry, Case Western Reserve University*
*10900 Euclid Avenue, Cleveland, OH 44106, USA*
*E-mail: genevieve.sauve@case.edu*
*https://caslabs.case.edu/sauve/*

*Supporting information and ORCID(s) from the author(s) for this article are available on the WWW under https://doi.org/10.1002/ejoc.201901736.*

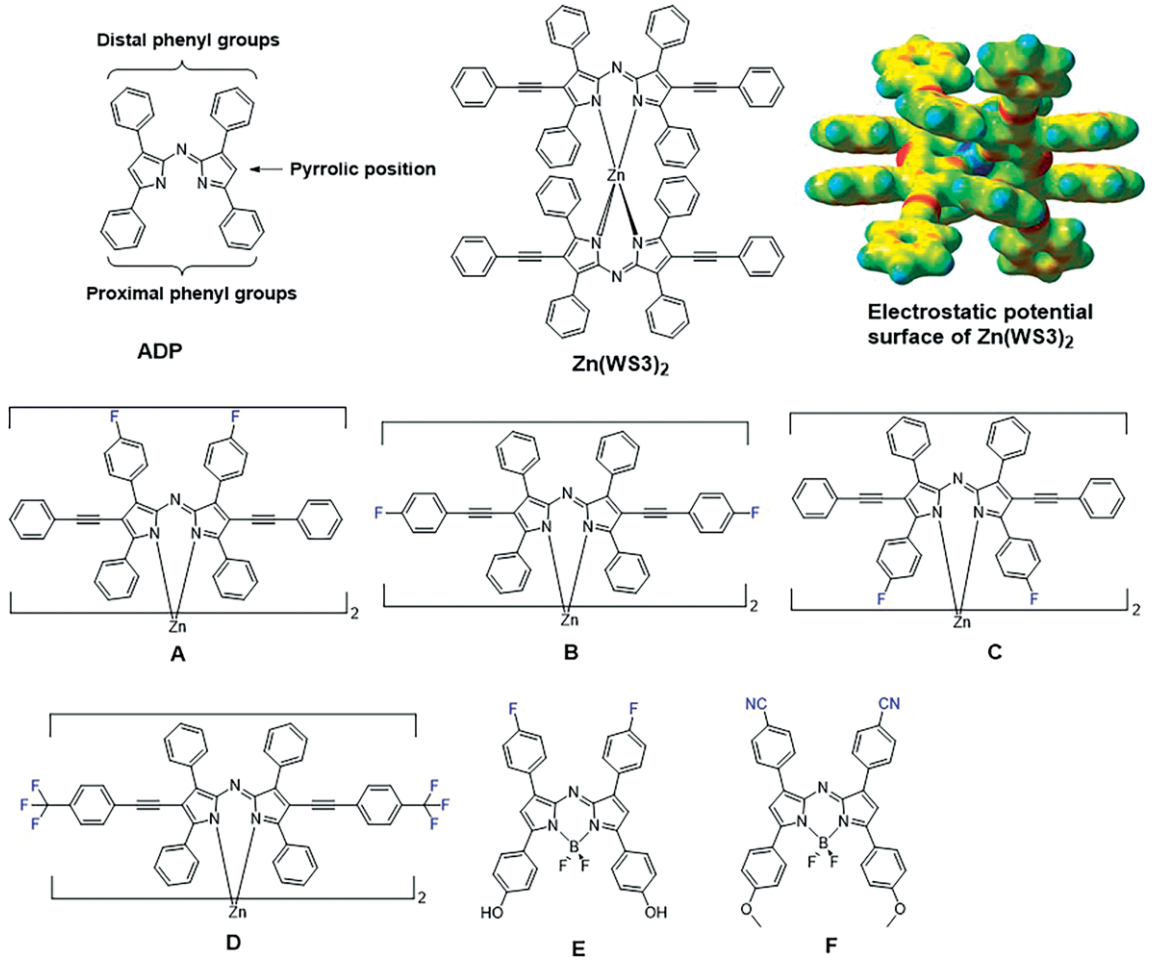


Figure 1. Structures of non-fullerene azadipyrromethene-based acceptors and examples of electron withdrawing group modifications to ADPs.

LUMO energy levels of the $BF_2^+$ chelate.[11] Our own DFT calculations had also shown that introducing nitrile groups at the *p*-pyrrolic phenylethynyl groups of $Zn(WS3)_2$ lowered the LUMO energy levels and increased electron affinity.[12] So far, these DFT predictions have not been verified by experiments.

Encouraged by these results, we synthesized ADP ligands with nitrile groups either at the *p*-distal phenyls or at the *p*-pyrrolic-phenylethynyls, Figure 2. The new ligands were coordinated with $Zn^{II}$, and $BF_2^+$. The optical, electrochemical and electrical properties of the new compounds are compared with those of un-substituted counterparts (Figure 2) to evaluate the effect of the nitrile groups. The potential of the nitrile-substituted zinc complexes as non-fullerene acceptors is also explored.

## Results and Discussion

### Synthesis

The synthesis of *p*-distally substituted ADP and its chelates, L1, $BF_2$(L1), and $Zn(L1)_2$, is shown in Scheme 1. Molecule 1 was obtained via an Aldol condensation reaction of 4-formylbenzonitrile and acetophenone using a published procedure in 65 % yield.[13] Molecule 2 was synthesized with the Michael addition reaction [Scheme 1(i)] in 82 % yield. Synthesis of ADP-based L1 was successfully prepared with ammonium acetate in 1-butanol giving a blue solid in 32 % yield. The $BF_2^+$ chelate, $BF_2$(L1), was obtained as a brown solid in 56 % yield. The chelation with $BF_2^+$ was confirmed by $^{19}F$ NMR, with a signal at –132.2 ppm. The zinc chelate of L1 was synthesized by reacting with sodium hydride and zinc chloride to give a blue solid 75 % yield.[6b] $Zn(L1)_2$ was purified by column chromatography, and its identity and purity were confirmed by MALDI-TOF MS, $^1H$ NMR, $^{13}C$ NMR, $^{19}F$ NMR, and elemental analysis.

The synthesis of ADP with cyanophenylethynyl pyrollic substituents, L2, and its chelate, $Zn(L2)_2$ is also shown in Scheme 1. We explored two coupling methods for installing the cyanophenylethynyls: Stille and Sonogarisha coupling. The Stille coupling method involved the reaction of iodinated ADP, 4, with 4-[(tributylstannyl)ethynyl]benzonitrile. However, the product contained impurities that could not be easily removed by solvent wash or by column chromatography. Part of the problem is that compound 4-[(tributylstannyl)ethynyl]benzonitrile is not stable. The Sonogashira coupling method, (v) in Scheme 1, was successful, giving the desired product L2 in 76 % yields. Chelation of L2 with $BF_2^+$ was attempted using the usual procedure, but the isolated yield was less than 1 % and insufficient for further characterization. The ligand L2 was treated with sodium hydride

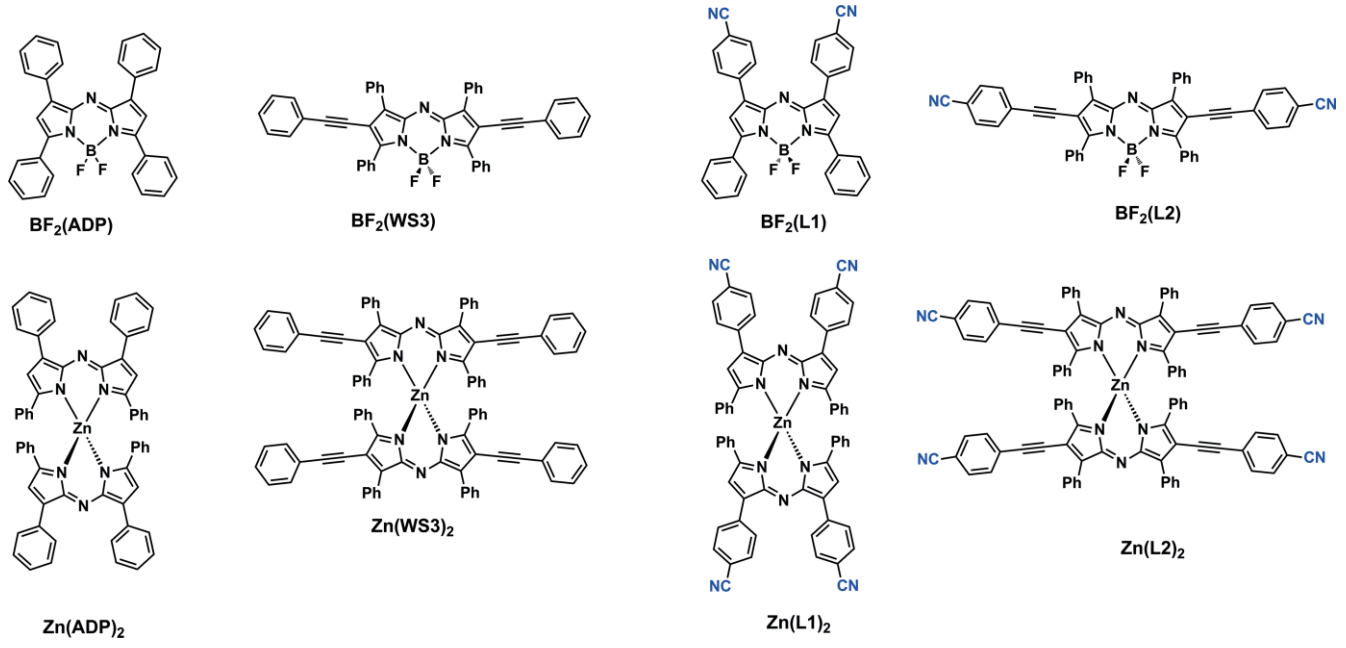


Figure 2. Structures of nitrile-substituted ADP chelates and their unsubstituted analogues.

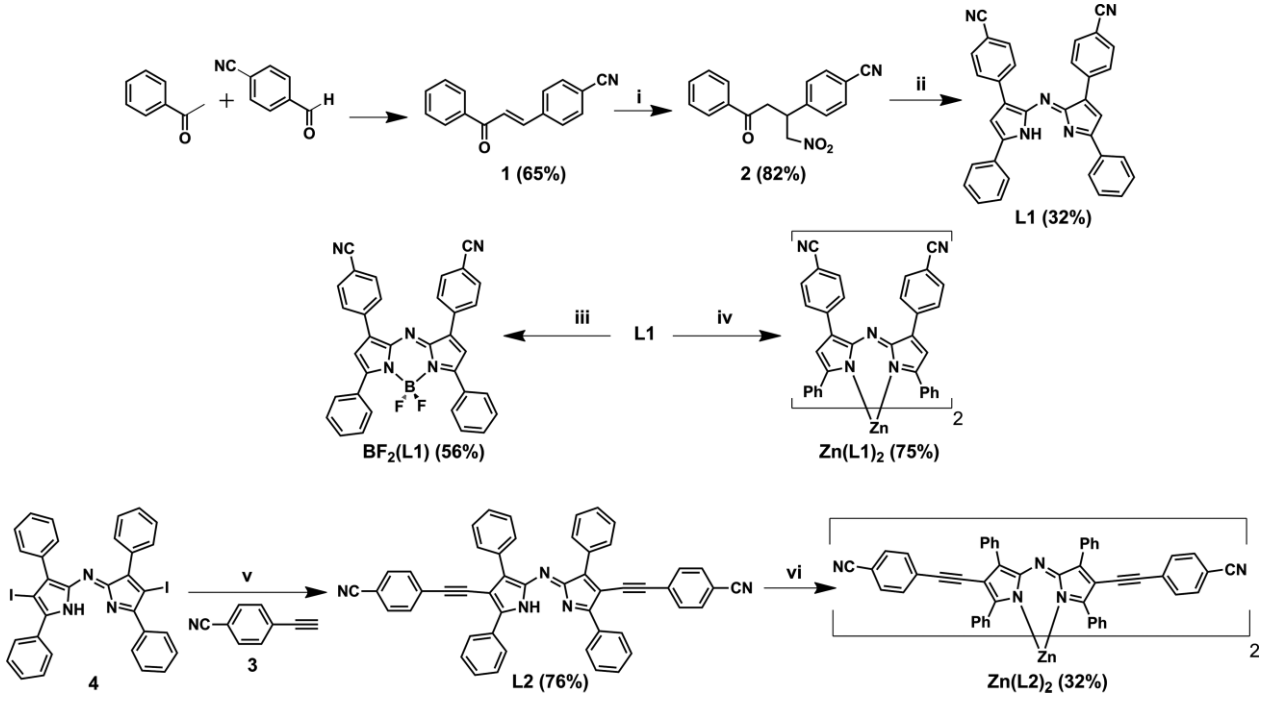


Scheme 1. Synthesis of $BF_2$(L1) and $Zn(L1)_2$. (i) $MeNO_2$, DIPEA, MeOH, reflux, 24 h, (ii) ammonium acetate, 1-butanol, reflux, 24 h, (iii) $BF_3/OEt_2$, DIPEA, DCM, 25 °C, 24 h, (iv) NaH, $ZnCl_2$, THF, reflux, 24 h for each reagent, (v) $Pd(PPh_3)_4$, xylenes, triethylamine, 70 °C, 36 h, (vi) NaH, $ZnCl_2$, THF, reflux, 24 h for each reagent.

and zinc chloride to form $Zn(L2)_2$. Most impurities could be removed by performing a simple Celite plug and a basic alumina plug. The final product was purified by silica gel chromatography to give a blue solid in 34 % yield. The identity of $Zn(L2)_2$ was confirmed by $^1H$ NMR, $^{13}C$ NMR, and MALDI-TOF MS.

Due to the addition of nitrile groups, $Zn(L1)_2$ and $Zn(L2)_2$ have lower solubility in all organic solvents than their un-substituted analogues $Zn(ADP)_2$ and $Zn(WS3)_2$, respectively. $Zn(L1)_2$ and $Zn(L2)_2$ tend to aggregate in most organic solvent such as acetone, methanol, THF and dimethylformamide. The solubility of $Zn(L1)_2$ is < 6 mg/mL in *o*-DCB and < 12 mg/mL in chloroform. $Zn(L2)_2$ is more soluble in organic solvent compared to that of $Zn(L1)_2$ due to the addition of phenylethynyl groups at the pyrrolic positions, which helps reduce self-aggregation.

$Zn(L2)_2$ has a solubility of > 12 mg/mL in *o*-DCB and > 20 mg/mL in chloroform.

## Optical Properties

Figure 3 shows the absorption and emission spectra of $BF_2$(L1) in chloroform, compared with that of $BF_2$(ADP) (also known at aza-BODIPY). *p*-nitrile substitution of the distal phenyls results in a red-shift of $\lambda_{max}$ by 14 nm to $\lambda_{max}$ = 666 nm and increase in the molar absorptivity from 50 $kM^{-1}$ $cm^{-1}$ for aza-BODIPY to 79 $kM^{-1}$ $cm^{-1}$ for $BF_2$(L1). The fluorescence quantum yield ($\Phi_f$) decreased with nitrile substitution, from 0.34 for aza-BODIPY to 0.21 for $BF_2$(L1). Jiao et al. synthesized similar materials (Figure 1F), but with methoxy groups in the *p*-proximal phenyls.[11] Upon nitrile substitution at the *p*-distal phenyl, they also observed a red-shift in the absorption spectrum (28 nm), and a decrease in $\Phi_f$.

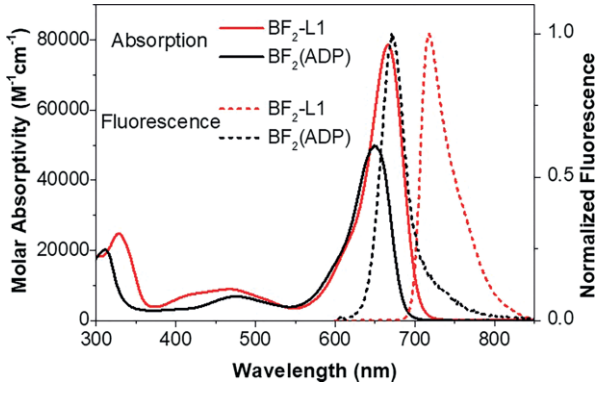


Figure 3. Absorption and fluorescence spectra of $BF_2$(ADP) and $BF_2$(L1) in chloroform.

The absorption spectra of $Zn(L1)_2$ and $Zn(L2)_2$ in solution and film are shown in Figure 4 and summarized in Table 1. The spectra of $Zn(ADP)_2$ and $Zn(WS3)_2$ are also included for comparison. The visible absorption spectra of the complexes are not greatly affected by the nitrile substitutions. The *p*-nitrile substitution on the distal phenyls red-shifts $\lambda_{max}$ by 14 nm, resulting in a $\lambda_{max}$ of 605 nm for $Zn(L1)_2$. On the other hand, nitrile substitution at the pyrrolic *p*-phenylethynyl position blue shifts $\lambda_{max}$ by 9 nm, from $\lambda_{max}$ = 674 nm for $Zn(WS3)_2$ to $\lambda_{max}$ = 665 nm for $Zn(L2)_2$. None of the zinc(II) complexes have detectable emissions. The visible absorption spectra trends are similar in films: distal phenyl substitution resulted in a red-shifted and broader absorption than $Zn(ADP)_2$ whereas pyrrolic substitution caused a small blue-shift compared to $Zn(WS3)_2$. Molecule $Zn(WS3)_2$ had the smallest optical gap (1.57 eV), followed by $Zn(L1)_2$ (1.59 eV), $Zn(L2)_2$ (1.62 eV), and $Zn(ADP)_2$ (1.65 eV). Figure S16 compares the solution and film spectra of zinc complexes. $Zn(L1)_2$ showed a 50 nm red-shift upon film formation, consistent with aggregation and solid-state π-interactions, whereas $Zn(L2)_2$ shows a much smaller red-shift of 17 nm, consistent with the pyrrolic substituents preventing aggregation. In comparison, $Zn(ADP)_2$ and $Zn(WS3)_2$ show similar changes going from solution to film than $Zn(L1)_2$ and $Zn(L2)_2$, respectively. The magnitude of the red-shift is therefore better correlated to the absence or presence of pyrrolic phenylethynyl groups than by the nitrile substitutions.

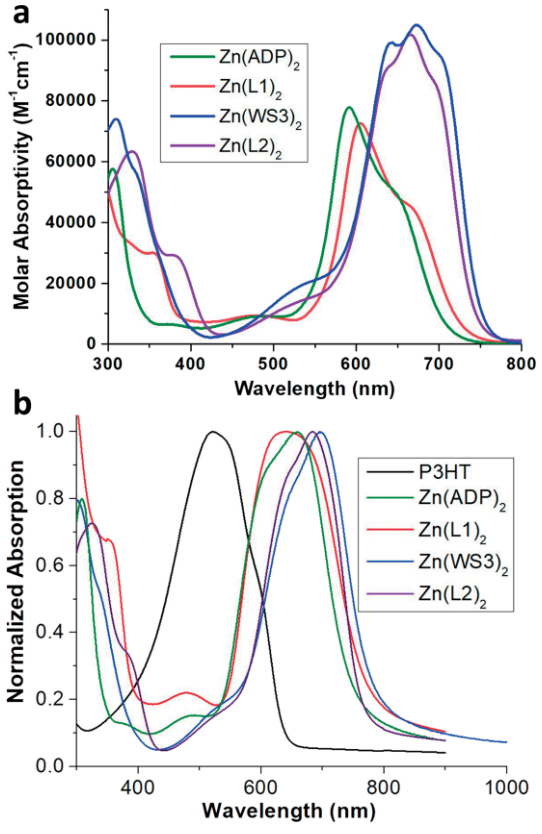


Figure 4. a) Absorption spectra of zinc(II) complexes in chloroform. b) Normalized absorption spectra of P3HT and zinc(II) chelated compounds in neat films. Films were spin-coated from chloroform solution and film thickness were ≈ 70 nm.

Table 1. Optical properties in chloroform solutions and neat films.[a]

| Material | Max.$\lambda^{abs}_{soln}$ [nm] [$\varepsilon$ ($kM^{-1}$ $cm^{-1}$)] | Max.$\lambda^{onset}_{soln}$ [nm] [$E_{g,opt}$ [eV]] | Max.$\lambda^{abs}_{film}$ [nm] | Max.$\lambda^{onset}_{film}$ [nm] [$E_{g,opt}$ [eV]] |
|---|---|---|---|---|
| P3HT | 453 [8.4] | 542 [2.29] | 521 | 636 [1.95] |
| $BF_2$(ADP) | 652 [50] | 687 [1.80] | –[â] | –[â] |
| $BF_2$(L1) | 666 [79] | 706 [1.76] | –[â] | –[â] |
| $Zn(ADP)_2$ | 591 [78] | 710 [1.75] | 659 | 753 [1.65] |
| $Zn(L1)_2$ | 605 [73] | 726 [1.71] | 641 | 779 [1.59] |
| $Zn(WS3)_2$ | 674 [105] | 755 [1.64] | 684 | 789 [1.57] |
| $Zn(L2)_2$ | 665 [102] | 748 [1.66] | 696 | 765 [1.62] |

[ â] Not able to obtain films on glass slides.

## Electrochemical Properties

The new chelates $BF_2$(L1), $Zn(L1)_2$ and $Zn(L2)_2$ were characterized by cyclic voltammetry in dichloromethane using $Fc/Fc^+$ as the internal standard, and their cyclic voltammograms are shown in Figure 5. All compounds exhibit two reversible reduction potentials. Both $BF_2$(ADP) and $BF_2$(L1) exhibit one reversible oxidation while the zinc complexes exhibit two reversible oxidations. The redox potentials, onsets, estimated HOMO/LUMO energy levels, and HOMO-LUMO gaps (or electronic gaps $E_{g,\ elect}$) are summarized in Table 2. The electrochemical data for

$BF_2$(ADP), $Zn(ADP)_2$ and $Zn(WS3)_2$ were included for comparison. With the addition of the nitrile groups, each of the new compounds exhibited an anodic shift in both first and second reduction potentials. For $BF_2$(L1), we observed the largest anodic shifts of 0.32 V for both the 1st and 2nd reductions. $Zn(L1)_2$ gives anodic shifts of 0.29 V and 0.25 V, while $Zn(L2)_2$ gives smaller anodic shifts of 0.16 V and 0.19 V for the 1st and 2nd reductions, respectively. In contrast, similar fluorine substitutions did not anodically shift the 1st reductions of the $Zn^{II}$ complexes within experimental error,[6b] demonstrating the superior ability of nitriles in tuning electron affinity. Nitrile substitution had a much larger effect on the 1st reduction potentials when installed at the *p*-distal phenyl than at the *p*-pyrrolic phenylethynyl position. The 1st oxidation potentials for $Zn(L1)_2$ and $Zn(L2)_2$ also exhibit anodic shifts of 0.19 V and 0.14 V compared to $Zn(ADP)_2$ and $Zn(WS3)_2$, respectively. The HOMO and LUMO energy levels were estimated from the 1st oxidation and 1st reduction onsets, respectively, and using the value of –4.8 eV for $Fc/Fc^+$ standard. As previously reported, the HOMO and LUMO energy levels for the $BF_2^+$ chelates were significantly deeper than those of the $Zn^{II}$ chelates. This is because the electron-deficient $BF_2^+$ lowers the HOMO and LUMO energy levels whereas DFT calculations suggest that $Zn^{II}$ does not participate in the frontier molecular orbitals of these complexes.[14] Both the HOMO and LUMO energy levels decreased with nitrile substitution and the HOMO-LUMO gap, or $E_{g,elec.}$, is in good agreement with the optical gap ($E_{g,opt}$, Table 1). The LUMO level of both $Zn(L1)_2$ and $Zn(L2)_2$ is very similar to the popular acceptor phenyl-C61-butyric acid ester (PCBM), estimated at –3.78 eV in our laboratory. Combined with deeper HOMOs, the new zinc complexes are promising candidates as electron acceptors in OPVs.

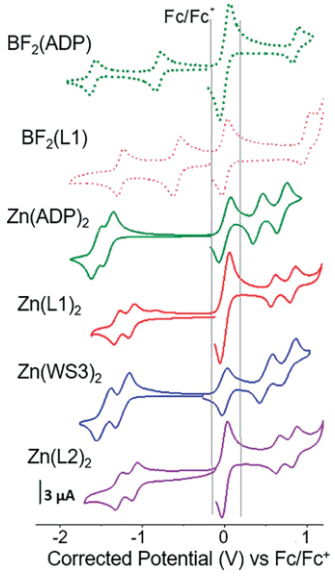


Figure 5. Cyclic voltammetry (CV) plots in 0.1 M $TBAPF_6$ dichloromethane solution, using $Fc/Fc^+$ as an internal standard.

## Fluorescence Quenching

To further evaluate the potential of our new ligands and chelates as acceptors for organic solar cells, we studied the optical properties of blends of our materials with the commonly studied donor, regioregular poly(3-hexylthiophene) (P3HT). The absorption spectra of P3HT:Zinc complex blend films (Figure S23) is broad, from 450 nm to ≈ 750–800 nm, due to the complementary absorption spectra of the zinc complexes with P3HT. $Zn(L2)_2$ was found to best complement the absorption spectra of P3HT, giving a film that absorbs to 800 nm. Figure 6 shows the emission spectra of P3HT and blends with zinc complexes. Since the zinc complexes do not emit, we are only probing the emission of P3HT. In all cases, the zinc complexes mostly quench the fluorescence of P3HT, consistent with electron or energy transfer from P3HT to the zinc complexes.

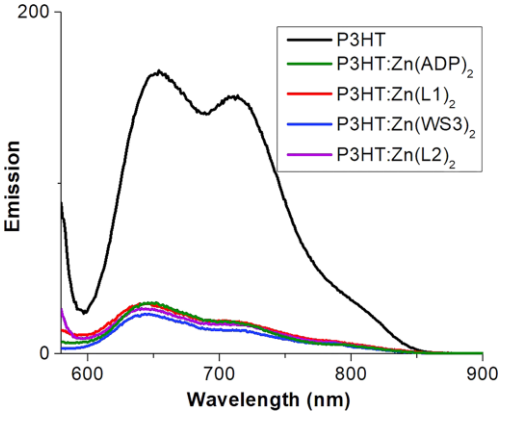


Figure 6. Fluorescence of P3HT ($\lambda_{ex}$ = 550 nm) in neat films and blend films with Zn chelated compounds.

Since the incomplete fluorescence quenching in film may be due to morphology, we also performed fluorescence quenching experiments in chloroform solution at various P3HT:Zinc complex ratios, shown in Figure S17–S20. Because the zinc complexes absorb light in the P3HT emission region, the emission

Table 2. Cyclic voltammetry data in dichloromethane solution.

| | $(E_{ox})^{1/2}$ [V] 1st ox. | 2nd ox. | $(E_{red})^{1/2}$ [V] 1st ox. | 2nd red. | $E_{onset}$ [V] 1st ox. | $E_{onset}$ [V] 1st red. | HOMO[a] [eV] | LUMO[a] [eV] (EA) | $E_{g,elect.}$ [eV] |
|---|---|---|---|---|---|---|---|---|---|
| $BF_2$(ADP) | 0.86 | NA | –0.90 | –1.60 | 0.77 | –0.73 | –5.57 | –4.07 | 1.5 |
| $BF_2$(L1) | 0.99 | NA | –0.58 | –1.27 | 0.92 | –0.53 | –5.72 | –4.27 | 1.45 |
| $Zn(ADP)_2$ | 0.40 | 0.69 | –1.42 | –1.56 | 0.34 | –1.33 | –5.14 | –3.47 | 1.67 |
| $Zn(L1)_2$ | 0.59 | 0.82 | –1.13 | –1.31 | 0.53 | –1.04 | –5.33 | –3.76 | 1.57 |
| $Zn(WS3)_2$ | 0.50 | 0.77 | –1.25 | –1.47 | 0.42 | –1.14 | –5.22 | –3.66 | 1.56 |
| $Zn(L2)_2$ | 0.64 | 0.85 | –1.09 | –1.28 | 0.56 | –0.99 | –5.36 | –3.81 | 1.55 |

[a] Calculated as: $-(E_{onset} + 4.8$ eV). EA is electron affinity.

spectra were corrected by taking inner filter effect into consideration.[14] The data from the corrected emission intensity vs. concentration of zinc complex was fitted to extract the Stern-Volmer constant $K_{sv}$. The quencher rate constant $K_q$ was calculated using the equation $K_q = K_{sv}/\tau$, where $\tau$ is fluorescence lifetime of P3HT and 500 ps in solution.[15] The results are summarized in Table 3. The quenching coefficient reflects electron accepting ability of the quencher if charge transfer is the only mechanism for fluorescence quenching. In this case, there may also be energy transfer. $Zn(L1)_2$ has a similar quenching coefficient ($56 \times 10^{12}$ $M^{-1}$ $S^{-1}$) than $Zn(ADP)_2$ ($58 \times 10^{12}$ $M^{-1}$ $S^{-1}$), suggesting that the addition of nitrile groups on the *p*-distal-phenyls does not affect charge transfer between P3HT and $Zn(ADP)_2$. The quenching coefficient of $Zn(L2)_2$ ($48 \times 10^{12}$ $M^{-1}$ $S^{-1}$) is 1.4 times larger than that of $Zn(WS3)_2$ ($34 \times 10^{12}$ $M^{-1}$ $S^{-1}$), suggesting that the addition of nitriles groups on the *p*-pyrrolic-phenylethynyl increases the charge accepting ability. Moreover, all Zn chelates exhibit larger quenching coefficients than PCBM ($32 \times 10^{12}$ $M^{-1}$ $S^{-1}$). The combination of optical and electrochemical properties of $Zn(L1)_2$ and $Zn(L2)_2$ make them promising acceptors for OPVs.

Table 3. Stern-Volmer quenching constants for Zn chelates and PCBM in P3HT solutions at 298K.[a]

| Compound | $K_{sv}$ [$\times 10^3$ $M^{-1}$] | $K_q$ [$\times 10^{12}$ $M^{-1}$ $S^{-1}$] | $R^2$ |
|---|---|---|---|
| $Zn(ADP)_2$ | 29 ± 2 | 58 | 0.993 |
| $Zn(L1)_2$ | 28 ± 1 | 56 | 0.993 |
| $Zn(WS3)_2$ | 17 ± 2 | 34 | 0.981 |
| $Zn(L2)_2$ | 24 ± 4 | 48 | 0.991 |
| PCBM[b] | 16[b] | 32 | 0.973[b] |

[a] Note: Three measurements were performed and $K_q$ was calculated from the average of $K_{SV}$. $R^2$ is the average correlation coefficient. [b] Published data.[14]

## Charge Carrier Mobilities

Charge carrier mobilities of zinc complexes were evaluated in neat films using the space-charge-limited-current (SCLC) method. No mobilities could be obtained for the $BF_2^+$ complex due to our inability to form good films. Measurements were obtained using the device structure ITO/PEDOT:PSS/Active layer/$MoO_3$/Ag for hole mobilities and ITO/ZnO/Active layer/Ca/Al for electron mobilities (see Figure S21). Charge carrier mobilities were extracted using the Mott–Gurney law under the trap free SCLCs situation $J = 9\varepsilon_r\varepsilon_0\mu V^2/(8L^3)$, where $J$ is the current, $\varepsilon_0$ is the permittivity of free space, $\varepsilon_r$ is the relative permittivity of the material, $\mu$ is the charge carrier mobility, $V$ is the effective voltage, and $L$ is the thickness of the active layer.[16] Results are summarized in Figure S21–S22 and Table 4. The electron mobility of $Zn(L1)_2$, $3.3 \times 10^{-5}$ $cm^2$ $V^{-1}$ $s^{-1}$, is three times higher than the electron mobility of $Zn(ADP)_2$, $1 \times 10^{-5}$ $cm^2$ $V^{-1}$ $s^{-1}$, and the electron mobility of $Zn(L2)_2$, $7.6 \times 10^{-5}$ $cm^2$ $V^{-1}$ $s^{-1}$, is three times higher than that of un-substituted $Zn(WS3)_2$, $1.4 \times 10^{-5}$ $cm^2$ $V^{-1}$ $s^{-1}$. On the other hand, hole mobility of $Zn(L2)_2$, $7 \times 10^{-5}$ $cm^2$ $V^{-1}$ $s^{-1}$, was slightly lower than the hole mobility of $Zn(WS3)_2$, $9.7 \times 10^{-5}$ $cm^2$ $V^{-1}$ $s^{-1}$, and the hole mobility of $Zn(L1)_2$, $4 \times 10^{-6}$ $cm^2$ $V^{-1}$ $s^{-1}$, was one magnitude order lower than that of $Zn(ADP)_2$. These results suggest that nitrile groups decrease hole mobility and increase electron mobility of zinc complexes.

Table 4. Charge carrier mobility by SCLC.

| Zn complexes | Neat Film $\mu_h$ [$cm^2$ $V^{-1}$ $s^{-1}$] | Neat Film $\mu_e$ [$cm^2$ $V^{-1}$ $s^{-1}$] |
|---|---|---|
| $Zn(ADP)_2$ | $4 \times 10^{-5}$ | $1 \times 10^{-5}$ |
| | $(3 \pm 1) \times 10^{-5}$ | $(9 \pm 2) \times 10^{-6}$ |
| $Zn(L1)_2$ | $4 \times 10^{-6}$ | $3.3 \times 10^{-5}$ |
| | $(3 \pm 1) \times 10^{-6}$ | $(2.5 \pm 0.9) \times 10^{-5}$ |
| $Zn(WS3)_2$ | $9.7 \times 10^{-5}$[b] | $1.4 \times 10^{-5}$[b] |
| $Zn(L2)_2$ | $7 \times 10^{-5}$ | $7.6 \times 10^{-5}$ |
| | $(6 \pm 1) \times 10^{-5}$ | $(7.4 \pm 0.2) \times 10^{-5}$ |

[a] Note: Four devices were made for each material and largest value and average value were reported. All films were made from *o*-DCB solvent. Film thicknesses for all devices were ≈ 70–80 nm. [b] Published data.[6a]

## Preliminary Results in OPVs

The zinc complexes were tested in OPVs using P3HT as the donor. We used the same fabrication conditions that worked well for $Zn(WS3)_2$. The current-voltage curves and performance parameters can be found in the supporting information section, Figure S24 and Table S1. The performance for the substituted zinc complexes were significantly lower than their corresponding un-substituted analogue, with a maximum power conversion efficiency of 0.30 % for $Zn(L1)_2$ and 0.11 % for $Zn(L2)_2$. To better understand these results, we estimated the charge carrier mobilities in blend films using the SCLC method and the results are summarized in Table S2. Hole mobility ranged from $1.8 \times 10^{-4}$ $cm^2$ $V^{-1}$ $s^{-1}$ to $6.7 \times 10^{-5}$ $cm^2$ $V^{-1}$ $s^{-1}$ and is attributed to charge transport in the P3HT phase. Since these numbers are lower than what we typically see in P3HT-based devices,[6a] we surmise that the P3HT self-assembly is not optimal in these blends. Likewise, the electron mobilities of the nitrile-substituted complexes are lower in blends than in neat films and are lower than in blends of the un-substituted analogues. These results point to unfavorable morphology in blend films. To confirm this, surface morphology of P3HT:zinc(II) complexes blend films were investigated by tapping-mode atomic force microscopy (AFM). The AFM phase and height images are shown in the Figure 7. The P3HT:$Zn(WS3)_2$ film has nano-fibrillar features with no signs of large scale aggregation and a roughness of 10.7 nm, consistent with our previously published data.[4a,6a] In contrast, P3HT:$Zn(L1)_2$ and P3HT:$Zn(L2)_2$ films do not clearly show the typical P3HT nanofibrils, which explains the relatively low hole mobilities observed. The P3HT:$Zn(L1)_2$ film shows segregated granular domains with an average size of 100 nm, which are assigned to $Zn(L1)_2$ aggregates. These aggregates are probably a consequence of $Zn(L1)_2$'s low solubility in organic solvents. The P3HT:$Zn(L2)_2$ film, on the other hand, has large segregated phases with a width around 210 nm and a high surface roughness of 18.2 nm. While the unfavorable film morphologies of P3HT:$Zn(L1)_2$ and P3HT:$Zn(L2)_2$ blend films can explain their low OPV performance, further experiments are needed to confirm. For example, future design of solution processable nitrile-based ADP chelates will include using alkyl solu-

bilizing groups,[4b,17] as alkyl solubilizing groups have been shown to facilitate solution processing as well as improve device properties of organic semiconductors.[18]

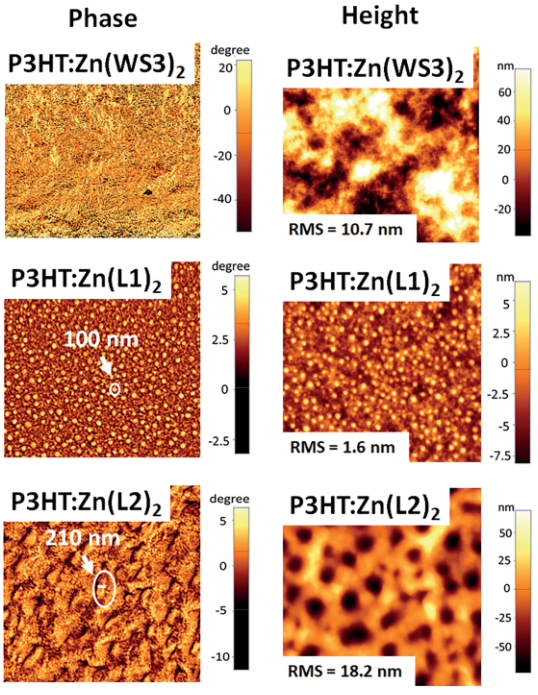


Figure 7. 5 × 5 μm AFM phase and height images for P3HT:Zn(WS3)$_2$, P3HT:Zn(L1)$_2$ and P3HT:Zn(L2)$_2$ blend films respectively. In phase images, dark and bright parts can be differentiated as different components. Roughness was shown on the phase images. The roughness calculated from 5 × 5 μm images follow the same trend as the roughness calculated from 1 × 1 μm images, Figure S25.

## Conclusion

We have synthesized new azadipyrromethene ligands substituted with nitrile groups and coordinated them with $BF_2^+$ and $Zn^{II}$. The substitution slightly red-shifts the visible absorption spectra of the $BF_2$(L1) and Zn(L1)$_2$, and slightly blue-shifts the absorption spectra of Zn(L2)$_2$ when compared to their un-substituted counterparts. Cyclic voltammetry experiments show that the nitrile substitutions anodically shift the reduction and oxidation potentials, leading to lower estimated HOMO and LUMO energy levels. Unlike fluorines, nitriles are therefore effective in lowering the energy levels of these types of complexes. Theoretical calculations are underway to better understand the effect of various substitutions on the energy levels of these types of complexes, including looking at the pi-donating/pi-accepting contributions. Fluorescence quenching experiments with P3HT are consistent with strong electron accepting properties for the new zinc complexes. SCLC data of neat films show that nitrile substitution enhances electron mobility. Preliminary tests in OPV using P3HT as the donor show photovoltaic responses, but unlike fluorine substitutions, nitrile substitutions were detrimental to OPV performance. One issue is that nitrile substitutions lower the complexes solubility and promote unfavorable morphology when blended with P3HT. Further work is required to fully establish the potential of nitrile substitution in the development of acceptors for OPV applications. Nevertheless, the ability to lower the energy levels of azadipyrromethene-based complexes using nitrile substitution may be useful for other applications of these dyes.

## Experimental Section

**Materials:** Acetophenone, 4- formylbenzonitrile, 4-ethynylbenzonitrile, nitromethane, diisopropylethylamine, ammonium acetate, $Pd(PPh_3)_4$, boron trifluoride etherate, sodium hydride, *n*-butyllithium, tributyltin chloride, and zinc chloride were bought from Sigma Aldrich and used as received. Dichloromethane (DCM) was distilled from calcium hydride and tetrahydrofuran (THF) was distilled from sodium wire and both solvents were stored in the refrigerator. All other solvents were obtained from Aldrich or Fisher Scientific. P3HT (MW = 20 kD, PDI = 1.3 in THF by GPC, polystyrene standard),,[19] 4-(3-oxo-3-phenylprop-1-en-1-yl)-benzonitrile (**2**),[13] (*E*)-chalcone, 2-benzyl-3-nitro-1-phenylpropan-1-one, azadipyrromethene,[20] (*Z*)-4-iodo-*N*-(4-iodo-3,5-diphenyl-2*H*-pyrrol-2-ylidene)-3,5-diphenyl-1*H*-pyrrol-2-amine (**4**),[21] and 4-[(tributylstannyl)ethynyl]benzonitrile[22] were made according to the literature.

**4-(1-Nitro-4-oxo-4-phenylbentan-2-yl)-benzonitrile (2):** 4-(3-oxo-3-phenylprop-1-en-1-yl)-benzonitrile (**1**) (1.0 g, 4.29 mmol), nitromethane (1.17 mL, 21.46 mmol), diisopropylethylamine (3.75 mL, 21.46 mmol) and 30 mL of methanol were added to a 50 mL round-bottomed flask with a reflux condenser and the mixture was stirred for 24 h at 65 °C. After cooling, the reaction was quenched by adding 10 mL of 1 M HCl solution slowly, causing the product to precipitate. The product was filtered and washed with cold methanol to obtain a light yellow solid. Yield: 1.03 g, 82 %. m.p. 136 °C. $^1$H NMR ($CDCl_3$): 7.91 (d, 2H, *J* = 7.3 Hz), 7.65 (d, 2H, *J* = 8.2 Hz), 7.59 (t, 1H, *J* = 7.4 Hz), 7.51–7.41 (m, 4H), 4.90–4.65 (m, 2H), 4.31 (m, 1H), 3.47 (m, 2H).

**1,9-Diphenyl-3,7-(4-cyanophenyl)azadipyrromethene (L1)**: 4-(1-nitro-4-oxo-4-phenylbentan-2-yl)-benzonitrile (**6**) (0.86 g, 2.93 mmol) and 45 equiv. of ammonium acetate (10.2 g, 0.13 mol) were dissolved in 1-butanol (20 mL) in a 50 mL round-bottomed flask with a reflux condenser. After refluxing for 24 h, the solvent was evaporated to obtain solid crude product. The crude product was washed with methanol and acetone, then filtered and dried to yield a dark blue solid. Yield: 0.23 g, 32 %. m.p. 330 °C. $^1$H NMR ($CDCl_3$): 8.09 (d, 4H, *J* = 8.4 Hz), 7.96 (d, 4H, *J* = 7.5 Hz), 7.71 (d, 4H, *J* = 7.7 Hz), 7.59–7.52 (m, 6H), 7.28 (s, 2H). MALDI-TOF MS: *m/z* calcd. for $[C_{34}H_{23}N_5]^-$ $[M]^-$ 498.18, found 498.28.

***N-N′*-Difluoroboryl-[1,9-diphenyl-3,7-(4-cyanophenyl)azadipyrromethene] {$BF_2$(L1)}**: 1,9-diphenyl-3,7-(4-cyanophenyl)azadipyrromethene (**L1**) (72 mg, 0.15 mmol) was dissolved in 15 mL of dry dichloromethane in flaks under $N_2$. Diisopropylethylamine (0.26 mL, 1.45 mmol) and boron trifluoride diethyl etherate (0.36 mL, 2.91 mmol) were added to the flask via syringe. The reaction was quench by adding 10 mL of water and followed by a liquid/liquid extraction with dichloromethane and water. The organic layer was dried with magnesium sulfate, and the solvent was evaporated. A silica gel plug was run in dichloromethane affording a brown solid. Yield: 44 mg, 56 %. $^1$H NMR ($CDCl_3$): 8.08 (d, 4H, *J* = 8.3 Hz), 8.06–8.02 (m, 4H), 7.76 (d, 4H, *J* = 8.2 Hz), 7.55–7.47 (m, 6H), 7.13 (s, 2H). $^{13}$C NMR ($CDCl_3$, ppm): 160.51, 145.63, 141.84, 136.27, 132.36, 131.67, 130.90, 129.75, 129.57, 128.86, 118.50, 112.90. $^{19}$F NMR ($CDCl_3$): −131.4 (q). MALDI-TOF MS: *m/z* calcd. for

$[C_{34}H_{22}N_5BF_2]^-$ $[M]^-$ 546.18, found 546.14. $C_{34}H_{20}BF_2N_5$ (547.18): calcd. C: 74.61, H: 3.68, N: 12.79, found C: 74.78, H: 3.89, N: 12.62.

**Bis[1,9-diphenyl-3,7-(4-cyanophenyl)azadipyrromethene]-zinc(II) {Zn(L1)$_2$}**: 1,9-diphenyl-3,7-(4-cyanophenyl)azadipyrromethene (**L1**) (100 mg, 0.20 mmol) was dissolved in 25 mL of dry THF in a flask under $N_2$. Sodium hydride (24 mg, 1 mmol) was added in one shot and the reaction was stirred at 60 °C for 24 h. Then, zinc chloride was added in one shot (42 mg, 0.3 mmol) and the reaction was allowed to proceed for and additional 24 h. The solvent was evaporated and the residue went through a Celite filter using dichloromethane to purify the product. The solution was concentrated under vacuum and the product was purified by silica gel chromatography in dichloromethane, yielding a blue solid. Yield: 80 mg, 75 %. $^1$H NMR ($CDCl_3$): 7.87 (d, 8H, $J$ = 8.3 Hz), 7.70 (d, 8H, $J$ = 8.3 Hz), 7.49–7.45 (m, 8H), 7.15–7.10 (m, 12H), 6.79 (s, 4H). $^{13}$C NMR ($CDCl_3$, ppm): 161.21, 147.98, 143.06, 138.25, 132.60, 131.87, 129.80, 128.30, 126.91, 119.00, 118.76, 111.28. MALDI-TOF MS: *m/z* calcd. for $[C_{68}H_{44}N_{10}Zn]^-$ $[M]^-$ 1060.27, found 1060.40. $C_{68}H_{40}N_{10}Zn$ (1060.27): calcd. C: 76.87, H: 3.79, N: 13.18, found C: 76.64, H: 3.49, N: 13.07.

**2,8-Di(4-cyanophenylacetylene)-1,3,7,9-tetraphenylazadipyrromethene (L2)**: 4-ethynylbenzonitrile (**3**) (0.3 g, 2.36 mmol) and 4-iodo-*N*-(4-iodo-3,5-diphenyl-2*H*-pyrrol-2-ylidene)-3,5-diphenyl-1*H*-pyrrol-2-amine (**4**), (0.75 g, 1.07 mmol) and were added in a 100 mL round-bottomed flask. Moisture and oxygen were removed by evacuating the flask and refilling with $N_2$. Distilled *m*-xylenes (30 mL) were added to dissolve the reactants. $Pd(PPh_3)_4$ (309 mg, 0.27 mmol) was added under $N_2$. 30 mL of triethylamine was added to the flask, and the reaction was heated to 70 °C for 48 h. After removing the flask from heat, the solvent was evaporated in vacuo. The residue was cooled in dry ice and vacuum filtered with 100 mL of methanol and 50 mL of dichloromethane. The product was obtained with 76 % yield and was utilized without further purification. M.p. > 350 °C. MALDI-TOF MS: *m/z* calcd. for $[C_{50}H_{29}N_5]^-$ $[M]^-$ 698.24, found 698.46.

**Bis[2,8-di(4-cyanophenylacetylene)-1,3,7,9-tetraphenylazadipyrromethene]zinc(II) {Zn(L2)$_2$}**: 2,8-di(4-cyanophenylacetylene)-1,3,7,9-tetraphenylazadipyrromethene (**L2**) (300 mg, 0.43 mmol) was added in a 100 mL round-bottomed flask. The flask was evacuated and refilled with $N_2$ three times to remove moisture and oxygen. The solid was dissolved with dry tetrahydrofuran (35 mL) and sodium hydride (24 mg, 1 mmol) was added in one shot. After 24 h, zinc chloride (64 mg, 0.44 mmol) was added to the reaction flask in one shot. The reaction continued for another 24 h. The solvent was evaporated and the residue was purified by filtering through a Celite filter using dichloromethane. The solution was concentrated under vacuum and the product was further purified by silica gel chromatography in dichloromethane, giving a blue solid. Yield: 100 mg, 32 %. m.p. 238 °C. $^1$H NMR ($CDCl_3$): 7.96–7.87 (m, 8H), 7.77–7.69 (m, 8H), 7.57 (d, 8H, $J$ = 8.7 Hz), 7.51–7.47 (m, 12H), 7.38 (d, 8H, $J$ = 8.3 Hz), 7.28–7.24 (m, 12H). $^{13}$C NMR ($CDCl_3$, ppm): 162.21, 146.90, 146.60, 132.60, 132.06, 131.92, 131.40, 130.85, 130.82, 130.39, 118.57, 111.24, 111.05, 95.20, 89.82, 89.77. MALDI-TOF MS: *m/z* calcd. for $[C_{100}H_{56}N_{10}Zn]^-$ $[M]^-$ 1460.40, found 1460.24. HRMS: calcd. for $[M + H]^+$ 1461.4054, found 1461.3996. $C_{100}H_{56}N_{10}Zn$ (1060.27): calcd. C: 82.10, H: 3.86, N: 9.57, found C: 81.87, H: 3.94, N: 9.61.

**General Methods:** $^1$H, $^{19}$F, and $^{13}$C spectra were recorded on a 500 MHz Bruker Ascend Avance III HD spectrometer at 25 °C. Chemical shifts ($^1$H) are reported in parts per million relative to relative to $Si(CH_3)_4$. Elemental analyses (C, H, and N) were performed using the optimum combustion conditions by Robertson Microlit Laboratories. Matrix-assisted laser desorption/ionization time-of-flight (MALDI-TOF) mass spectra were measured on a Bruker Autoflex III MALDI-TOF MS and samples were prepared from chloroform solutions using a 2,2′:5′,2″-terthiophene matrix. MALDI-TOF MS spectra were acquired in reflective negative mode on a Bruker Autoflex III smartbean MALDI-TOF/TOF spectrometer. UV/Visible absorption spectra were collected on an Agilent Cary 5000 Vis-UV-NIR spectrophotometer in HPLC grade chloroform. Fluorescence spectra were recorded using an Agilent Eclipse fluorescence spectrometer and excitation wavelength was 550 nm for all films. Spin coating of films was performed with a Laurell Spin Coater WS-650. All films for UV/Vis spectroscopy were prepared from $1.0 \times 10^{-2}$ mM solution in HPLC chloroform. The solutions were filtered through a 0.45 μm PTFE filter, then spun-cast on glass at 400 rpm for 40 seconds. Fluorescence quenching experiments were performed with blended films of P3HT:Zn chelates in a 1:1 (wt:wt) ratio with concentration of 10 mg/mL in HPLC chloroform. The solutions were filtered through a 0.45 μm PTFE filter, then spun-cast on glass at 400 rpm for 40 seconds. Cyclic voltammetry experiments were conducted using an Auto-Lab-PGSTAT 302N, Eco Chemie potentiostat at room temperature. A typical three-electrode configuration was used with a glassy carbon electrode as the working electrode and two platinum wires as the counter and pseudoreference electrodes. Ferrocene/ferrocenium was used as the internal standard. The measurements were performed with a scan rate of 0.1 V/s in degassed DCM with tetra-*n*-butylammonium hexafluorophosphate (0.1 M TBAPF) as the supporting electrolyte. The electrolyte solution was purged with nitrogen ($N_2$) for 5 min prior to each measurement. Thermal gravimetric analysis (TGA) was performed on a TA instrument Q500 thermogravimetric analyzer. Weight loss were recorded by heating samples from 25 °C to 800 °C at a heating scan rate of 10 °C/min. Fluorescence quenching. Fluorescence and absorption spectra of P3HT were measured as function of varied concentration of Zn chelates. The concentration of P3HT was 3 mg/mL and the concentration of Zn chelated varied from 0 μM to 12 μM. The excitation wavelength was 455 nm. Emission spectra were corrected for the inner filter effect and the corrected emission intensity were used to analize Stern-Volmer equation according to the published procedures.[14] Stern-Volmer equation: $E_0/E = K_{sv}[Q] + 1 = K_q\tau[Q] + 1$, where $E_0$ is the corrected emission intensity of P3HT at 570 nm and $E$ is the corrected emission intensity of P3HT with varied concentration of quencher at 570 nm. $K_{sv}$ is the Stern-Volmer constant and [Q] is the quencher concentration; $K_q$ is the quencher rate coefficient and $\tau$ is the fluorescence lifetime of P3HT in solution.

For single-carrier device fabrication, ITO-coated glass substrates were cleaned stepwise in soapy water, DI water, acetone and 2-propanol under ultrasonication for 15 minutes followed to a Reactive Ion Etcher (RIE) treatment for 30 seconds. Hole-only devices had the device structure: ITO/PEDOT:PSS/active layer/$MoO_3$/Ag. The PEDOT:PSS layer was prepared by filtering a water solution of 1.3 wt.-% PEDOT:PSS through a 0.45 μm PTFE filter followed by spin coating at 4000 rpm for 60 seconds and heated at 150 °C for 10 minutes. The photoactive layers were spin coated inside the glovebox at 1000 rpm for 40 seconds followed by 2000 rpm for 2 seconds from a blend solution with a total concentration of 20 mg/mL in *o*-DCB (*o*-dichlorobenzene). The solutions were filtered through a 0.45 μm PTFE filter prior to spin coating. All acceptors were blended with P3HT in a 1:0.7 ratio. All active layers were made from *o*-DCB solution. The active layer thicknesses were about 85 nm. The photoactive layers were pre-annealed at 120 °C for 30 minutes followed by thermal deposition of $MoO_3$ (10 nm) and Ag (80 nm) using the Angstrom Engineering Evovac Deposition System. For electron-only devices with an ITO/ZnO/active layer/Ca/Al structure, cleaning of

the ITO substrate, ZnO film and active layer film formation was performed as described previously. Calcium (30 nm) and Al (100 nm) were thermally deposited. Dark current measurements were performed using a Keithley 2400 source meter inside the glovebox. The devices have a total effective area of 0.20cm$^2$. For solar cell fabrication, inverted structure (ITO/ZnO/P3HT:Acceptor/$MoO_3$/Ag) was used for all devices. ITO-coated glass substrates cleaning, ZnO layer, $MoO_3$ layer, and Ag layer were prepared by the same procedure mentioned in the charge-carrier device fabrication. Active layer was prepared from a 1:0.7 weight ratio of P3HT: Acceptor with blend concentration of 20 mg/mL in *o*-DCB solution by spin coating at 1000 rpm for 40 seconds and followed by 2000 rpm for 2 seconds. All solutions were filtered through 0.45 μm PTFE filters prior to spin coating. The photoactive layers were annealed at 120 °C for 30 minutes before $MoO_3$ deposition. Film thickness were measured by using a KLA-Tencor P6 stylus profilometer. Scratches were made on the surface of the device to remove film in a small area. Film thickness measurement was taken from the height between the scratched area and the intact film area. Three measurements were made across the diagonal for each film. Tapping-mode atomic force microscopy (AFM) was performed on blend films using a Park NX 10 Atomic Force Microscope (XEP 3.0.4 Build 37). The acquired images were processed and analyzed using XEI (1.8.0, Build 36).

## Acknowledgments

This work was supported by the National Science Foundation [CHEM 1148652]. We also thank Peiran Wei and Dr. Pentzer for AFM measurements and for providing access to UV/Vis instrument, Dr. John D. Protasiewicz for facilitating cyclic voltammetry, and Dr. Ina Martin and the Materials for Optoelectronics Research and Education (MORE) Center at CWRU for help and instrumentation related to devices. This material is based upon work supported by the National Science Foundation under Grant MRI-28.5 0821515 (for the purchase of the MALDI–TOF–TOF).

**Keywords:** Cyano group · Aza-BODIPY · Pi acceptor · Organic solar cell · Non-fullerene acceptors

[1] a) A. Loudet, K. Burgess, *Chem. Rev.* **2007**, *107*, 4891–4932; b) D. Partyka, N. Deligonul, M. Washington, T. Gray, *Organometallics* **2009**, *28*, 5837–5840.
[2] a) A. Palma, J. F. Gallagher, H. Mueller-Bunz, J. Wolowska, E. J. L. McInnes, D. F. O'Shea, *Dalton Trans.* **2009**, 273–279; b) Y. Ge, D. F. O'Shea, *Chem. Soc. Rev.* **2016**, *45*, 3846–3864.
[3] a) T. Mueller, R. Gresser, K. Leo, M. Riede, *Sol. Energy Mater. Sol. Cells* **2012**, *99*, 176–181; b) S. Y. Leblebici, L. Catane, D. E. Barclay, T. Olson, T. L. Chen, B. Ma, *ACS Appl. Mater. Interfaces* **2011**, *3*, 4469–4474; c) X. Zhang, Y. Zhang, L. Chen, Y. Xiao, *RSC Adv.* **2015**, *5*, 32283–32289; d) M. Lorenz-Rothe, K. S. Schellhammer, T. Jaegeler-Hoheisel, R. Meerheim, S. Kraner, M. P. Hein, C. Schuenemann, M. L. Tietze, M. Hummert, F. Ortmann, G. Cuniberti, C. Koerner, K. Leo, *Adv. Electron. Mater.* **2016**, *2*, 1600152; e) K. S. Schellhammer, T.-Y. Li, O. Zeika, C. Koerner, K. Leo, F. Ortmann, G. Cuniberti, *Chem. Mater.* **2017**, *29*, 5525–5536.
[4] a) Z. Mao, W. Senevirathna, J. Y. Liao, J. Gu, S. V. Kesava, C. Guo, E. D. Gomez, G. Sauvé, *Adv. Mater.* **2014**, *26*, 6290–6294; b) C. Wang, P. Wei, J. H. L. Ngai, A. L. Rheingold, T. G. Gray, Y. Li, E. Pentzer, R. Li, L. Zhu, G. Sauvé, *J. Mater. Chem. A* **2019**, *7*, 24614–24625.
[5] G. Sauvé, R. Fernando, *J. Phys. Chem. Lett.* **2015**, *6*, 3770–3780.
[6] a) S. Pejić, A. M. Thomsen, F. S. Etheridge, R. Fernando, C. Wang, G. Sauvé, *J. Mater. Chem. C* **2018**, *6*, 3990–3998; b) F. S. Etheridge, R. J. Fernando, S. Pejić, M. Zeller, G. Sauvé, *Beilstein J. Org. Chem.* **2016**, *12*, 1925–1938.
[7] A. N. Amin, M. E. El-Khouly, N. K. Subbaiyan, M. E. Zandler, M. Supur, S. Fukuzumi, F. D'Souza, *J. Phys. Chem. A* **2011**, *115*, 9810–9819.
[8] a) R. Ragni, A. Punzi, F. Babudri, G. M. Farinola, *Eur. J. Org. Chem.* **2018**, *2018*, 3500–3519; b) Q. Zhang, M. A. Kelly, N. Bauer, W. You, *Acc. Chem. Res.* **2017**, *50*, 2401–2409; c) F. Babudri, G. Farinola, F. Naso, R. Ragni, *Chem. Commun.* **2007**, 1003–1022.
[9] T. X. Carroll, T. D. Thomas, H. Bergensen, K. J. Børve, L. J. Sæthre, *J. Org. Chem.* **2006**, *71*, 1961–1968.
[10] Y. F. Lim, Y. Shu, S. R. Parkin, J. E. Anthony, G. G. Malliaras, *J. Mater. Chem.* **2009**, *19*, 3049–3056.
[11] L. Jiao, Y. Wu, S. Wang, X. Hu, P. Zhang, C. Yu, K. Cong, Q. Meng, E. Hao, M. G. H. Vicente, *J. Org. Chem.* **2014**, *79*, 1830–1835.
[12] W. Senevirathna, C. M. Daddario, G. Sauvé, *J. Phys. Chem. Lett.* **2014**, *5*, 935–941.
[13] K. D. Ashtekar, R. J. Staples, B. Borhan, *Org. Lett.* **2011**, *13*, 5732–5735.
[14] W. Senevirathna, G. Sauve, *J. Mater. Chem. C* **2013**, *1*, 6684–6694.
[15] B. Ferreira, P. F. da Silva, J. S. Seixas de Melo, J. Pina, A. Macanita, *J. Phys. Chem. B* **2012**, *116*, 2347–2355.
[16] a) N. A. Unlu, S. O. Hacioglu, G. Hizalan, D. E. Yildiz, L. Toppare, A. Cirpan, *J. Electrochem. Soc.* **2017**, *164*, G71–G76; b) J. C. Blakesley, F. A. Castro, W. Kylberg, G. F. A. Dibb, C. Arantes, R. Valaski, M. Cremona, J. S. Kim, J.-S. Kim, *Org. Electron.* **2014**, *15*, 1263–1272.
[17] a) W. Sheng, Y.-Q. Zheng, Q. Wu, Y. Wu, C. Yu, L. Jiao, E. Hao, J.-Y. Wang, J. Pei, *Org. Lett.* **2017**, *19*, 2893–2896; b) W. Sheng, F. Chang, Q. Wu, E. Hao, L. Jiao, J. Y. Wang, J. Pei, *Org. Lett.* **2020**, *22*, 185–189.
[18] a) D. Ho, R. Ozdemir, H. Kim, T. Earmme, H. Usta, C. Kim, *ChemPlusChem* **2019**, *84*, 18-37; b) C. B. Nielsen, M. Turbiez, I. McCulloch, *Adv. Mater.* **2013**, *25*, 1859–1880.
[19] M. Jeffries-El, G. Sauve, R. McCullough, *Macromolecules* **2005**, *38*, 10346–10352.
[20] A. Gorman, J. Killoran, C. O'Shea, T. Kenna, W. M. Gallagher, D. F. O'Shea, *J. Am. Chem. Soc.* **2004**, *126*, 10619–10631.
[21] L. Gao, W. Senevirathna, G. Sauve, *Org. Lett.* **2011**, *13*, 5354–5357.
[22] B. P. Warner, S. L. Buchwald, *J. Org. Chem.* **1994**, *59*, 5822–5823.

Received: November 25, 2019